Ultrahigh resolution optical coherence tomography and pancorrection for cellular imaging of the living human retina

Enrique J. Fernández[1,2,3], Boris Hermann[1,3], Boris Považay[1,3], Angelika Unterhuber[1,3], Harald Sattmann[3], Bernd Hofer[1,3], Peter K. Ahnelt[4], Wolfgang Drexler[1,3]*

[1]*Biomedical Imaging Group, School of Optometry and Vision Sciences, Cardiff University, Wales, UK*
[2]*Laboratorio de Óptica, Centro de Investigación en Óptica y Nanofísica, Universidad de Murcia, Campus de Espinardo, E-30071 Murcia, Spain*
[3]*Center of Biomedical Engineering and Physics, Vienna University of Medicine, Austria*
[4]*Center for Physiology and Pathophysiology, Vienna University of Medicine, Austria*
[*]*Corresponding author: wdrexler@cardiff.ac.uk*

Abstract: Cellular *in vivo* visualization of the three dimensional architecture of individual human foveal cone photoreceptors is demonstrated by combining ultrahigh resolution optical coherence tomography and a novel adaptive optics modality. Isotropic resolution in the order of 2-3μm, estimated from comparison with histology, is accomplished by employing an ultrabroad bandwidth Titanium:sapphire laser with 140nm bandwidth and previous correction of chromatic and monochromatic ocular aberrations. The latter, referred to as pancorrection, is enabled by the simultaneous use of a specially designed lens and an electromagnetically driven deformable mirror with unprecedented stroke for correcting chromatic and monochromatic aberrations, respectively. The increase in imaging resolution allows for resolving structural details of distal elements of individual foveal cones: inner segment zones - myoids and ellipsoids - are differentiated from outer segments protruding into pigment epithelial processes in the retina. The presented technique has the potential to unveil photoreceptor development and pathogenesis as well as improved therapy monitoring of numerous retinal diseases.

OCIS codes: (010.1080) Adaptive optics; (170.4500) Optical coherence tomography; (330.4460) Ophthalmic optics; (330.5370) Physiological optics; (110.6955) Tomographic imaging.

References and links

1. H. R. Taylor and J. E. Keeffe, "World blindness: a 21st century perspective," Br. J. Ophthalmol. **85**, 261-266 (2001).
2. J. Porter, A. Guirao, I. Cox, and D. R. Williams, "Monochromatic aberrations of the human eye in a large population," J. Opt. Soc. Am. A **18**, 1793–1803 (2001).
3. F. J. Castejón-Mochón, N. López-Gil, A. Benito, and P. Artal, "Ocular wavefront aberration statistics in a normal young population," Vision Res. **42**, 1611–1617 (2002).
4. D. Huang, E. A. Swanson, C. P. Lin, J. S. Schuman, W. G. Stinson, W. Chang, M. R. Hee, T. Flotte, K. Gregory, C. A. Puliafto, and J. G. Fujimoto, "Optical coherence tomography," Science **254**, 1178-1181 (1991).
5. W. Drexler, U. Morgner, F. X. Kärtner, C. Pitris, S. A. Boppart, X. D. Li, E. P. Ippen, and J. G. Fujimoto, "In vivo ultrahigh-resolution optical coherence tomography," Opt. Lett. **24**, 1221-1223 (1999).
6. W. Drexler, U. Morgner, R. K. Ghanta, F. X. Kaertner, J. S. Schuman, and J. G. Fujimoto, "Ultrahigh resolution ophthalmic optical coherence tomography," Nature Med. **7**, 502-507 (2001).
7. W. Drexler, H. Sattmann, B. Hermann, T. H. Ko, M. Stur, A. Unterhuber, C. Scholda, O. Findl, M. Wirtitsch, J. G. Fujimoto, and A. F. Fercher, "Enhanced visualization of macular pathology using ultrahigh resolution optical coherence tomography," Arch. Ophthalmol. **121**, 695-706 (2003).

#96661 - $15.00 USD Received 27 May 2008; revised 6 Jul 2008; accepted 7 Jul 2008; published 9 Jul 2008

8. T. H. Ko, J. G. Fujimoto, J. S. Duker, L. A. Paunescu, W. Drexler, C. R. Baumal, C. A. Puliafito, E. Reichel, A. H. Rogers, and J. S. Schuman, "Comparison of ultrahigh and standard resolution optical coherence tomography for imaging macular hole pathology and repair," Ophthalmology **111**, 2033-2043 (2004).
9. B. Hermann, E. J. Fernández, A. Unterhuber, H. Sattmann, A. F. Fercher, W. Drexler, P. M. Prieto, and P. Artal, "Adaptive-optics ultrahigh-resolution optical coherence tomography," Opt. Lett. **29**, 2142-2144 (2004).
10. F. Fercher, C. K. Hitzenberger, G. Kamp, and S.Y. El-Zaiat, "Measurement of intraocular distances by backscattering spectral interferometry," Opt. Comm. **117**, 43-48 (1995).
11. M. A. Choma, M. V. Sarunic, C.H. Yang, and J. A. Izatt, "Sensitivity advantage of swept source and Fourier domain optical coherence tomography," Opt. Express **11**, 2183-2189 (2003), http://www.opticsinfobase.org/abstract.cfm?URI=oe-11-18-2183
12. M. Wojtkowski, R. A. Leitgeb, A. Kowalczyk, T. Bajraszewski, and A. F. Fercher, "In-vivo human retinal imaging by Fourier domain optical coherence tomography," J. Biomed. Opt. **7**, 457-463 (2002).
13. R. Leitgeb, C. Hitzenberger, and A. Fercher, "Performance of fourier domain vs. time domain optical coherence tomography," Opt. Express **11**, 889-894 (2003), http://www.opticsinfobase.org/abstract.cfm?URI=oe-11-8-889.
14. J. F. de Boer, B. Cense, B. H. Park, M. C. Pierce, G. J. Tearney, and B. E. Bouma, "Improved signal-to-noise ratio in spectral-domain compared with time-domain optical coherence tomography," Opt. Lett. **28**, 2067-2069 (2003).
15. Y. Zhang, J. Rha, R. Jonnal, and D. Miller, "Adaptive optics parallel spectral domain optical coherence tomography for imaging the living retina," Opt. Express **13**, 4792-4811 (2005), http://www.opticsinfobase.org/abstract.cfm?URI=oe-13-12-4792.
16. R. Zawadzki, S. Jones, S. Olivier, M. Zhao, B. Bower, J. Izatt, S. Choi, S. Laut, and J. Werner, "Adaptive-optics optical coherence tomography for high-resolution and high-speed 3D retinal in vivo imaging," Opt. Express **13**, 8532-8546 (2005), http://www.opticsinfobase.org/abstract.cfm?URI=oe-13-21-8532.
17. E. J. Fernández, B. Považay, B. Hermann, A. Unterhuber, H. Sattmann, P. M. Prieto, R. Leitgeb, P. Ahnelt, P. Artal, and W. Drexler, "Three dimensional adaptive optics ultrahigh-resolution optical coherence tomography using a liquid crystal spatial light modulator," Vision Res. **45**, 3432-3444 (2005).
18. Y. Zhang, B. Cense, J. Rha, R. S. Jonnal, W. Gao, R. J. Zawadzki, J. S. Werner, S. Jones, S. Olivier, and D. T. Miller, "High-speed volumetric imaging of cone photoreceptors with adaptive optics spectral-domain optical coherence tomography," Opt. Express **14**, 4380-4394 (2006), http://www.opticsinfobase.org/abstract.cfm?URI=oe-14-10-4380.
19. R. J. Zawadzki, S. Choi, S. M. Jones, S. Oliver, and J. S. Werner, "Adaptive optics-optical coherence tomography: optimizing visualization of microscopic retinal structures in three dimensions," J. Opt. Soc. Am. A **24**, 1373-1383 (2007).
20. D. Merino, C. Dainty, A. Bradu, and A. G. Podoleanu, "Adaptive optics enhanced simultaneous en-face optical coherence tomography and scanning laser ophthalmoscopy," Opt. Express **14**, 3345-3353 (2006), http://www.opticsinfobase.org/abstract.cfm?URI=oe-14-8-3345.
21. C. E. Bigelow, N. V. Iftimia, R. D. Ferguson, T. E. Ustun, B. Bloom, and D. X. Hammer, "Compact multimodal adaptive-optics spectral-domain optical coherence tomography instrument for retinal imaging," J. Opt. Soc. Am. A **24**, 1327-1336 (2007).
22. M. Pircher, R. J. Zawadzki, J. W. Evans, J. S. Werner, and C. K. Hitzenberger, "Simultaneous imaging of human cone mosaic with adaptive optics enhanced scanning laser ophthalmoscopy and high-speed transversal scanning optical coherence tomography," Opt Lett. **33**, 22-24 (2008).
23. E. J. Fernández and W. Drexler, "Influence of ocular chromatic aberration and pupil size on transverse resolution in ophthalmic adaptive optics optical coherence tomography," Opt. Express **13**, 8184-8197 (2005), http://www.opticsinfobase.org/abstract.cfm?URI=oe-13-20-8184.
24. E. J. Fernández, A. Unterhuber, B. Považay, B. Hermann, P. Artal, and W. Drexler, "Chromatic aberration correction of the human eye for retinal imaging in the near infrared," Opt. Express **14**, 6213-6225 (2006), http://www.opticsinfobase.org/abstract.cfm?URI=oe-14-13-6213.
25. E. J. Fernández, L. Vabre, B. Hermann, A. Unterhuber, B. Povazay, and W. Drexler, "Adaptive optics with a magnetic deformable mirror: applications in the human eye," Opt. Express **14**, 8900-8917 (2006), http://www.opticsinfobase.org/abstract.cfm?URI=oe-14-20-8900.
26. P. M. Prieto, F. Vargas-Martín, S. Goelz, and P. Artal, "Analysis of the performance of the Hartmann-Shack sensor in the human eye," J. Opt. Soc. Am. A **17**, 1388-1398 (2000).
27. J. Liang, B. Grimm, S. Goelz, and J. F. Bille, "Objective measurement of wave aberrations of the human eye with use of a Hartmann-Shack wave-front sensor," J. Opt. Soc. Am. A **11**, 1949-1955 (1994).
28. E. J. Fernández and P. Artal, "Membrane deformable mirror for adaptive optics: performance limits in visual optics," Opt. Express **11**, 1056-1069 (2003), http://www.opticsinfobase.org/abstract.cfm?URI=oe-11-9-1056.
29. E. J. Fernández, A. Unterhuber, P. Prieto, B. Hermann, W. Drexler, and P. Artal, "Ocular aberrations as a function of wavelength in the near infrared measured with a femtosecond laser," Opt. Express **13**, 400-409 (2005), http://www.opticsinfobase.org/abstract.cfm?URI=oe-13-2-400.

#96661 - $15.00 USD Received 27 May 2008; revised 6 Jul 2008; accepted 7 Jul 2008; published 9 Jul 2008

30. Unterhuber, B. Povazay, B. Hermann, H. Sattmann, W. Drexler, V. Yakovlev, G. Tempea, C. Schubert, E. M. Anger, P. K. Ahnelt, M. Stur, J. E. Morgan, A. Cowey, G. Jung, T. Le, and A. Stingl, "Compact, low-cost TiAl2O3 laser for in vivo ultrahigh-resolution optical coherence tomography," Opt. Lett. **28**, 905-907 (2003).
31. ANSI Z 136.1, *Safe Use of Lasers*, (American National Standard Institute, New York, 2000).
32. W. Krebs and I. Krebs, *Primate Retina and Choroid: Atlas of Fine Structure in Man and Monkey*, (Springer Verlag, New York, 1991).
33. Q. V. Hoang, R. A. Linsenmeier, C. K. Chung, and C. A. Curcio, "Photoreceptor inner segments in monkey and human retina: mitochondrial density, optics, and regional variation," Vis. Neurosci. **19**, 395-407 (2002).
34. N. W. Roberts, "The optics of vertebrate photoreceptors: anisotropy and form birefringence," Vision Res. **46**, 3259-3266(2006).
35. C. A. Curcio, K. R. Sloan, R. E. Kalina, and A. E. Hendrickson, "Human photoreceptor topography," J. Comp. Neurol. **292**, 497-523 (1990).
36. B. Borwein, D. Borwein, J. Medeiros, and J. W. McGowan, "The ultrastructure of monkey foveal photoreceptors, with special reference to the structure, shape, size, and spacing of the foveal cones," Am. J. Anat. **159**, 125-146 (1980).
37. Roorda and D. R. Williams, "Optical fiber properties of individual human cones," J. Vis. **2**, 404-412 (2002).
38. R. H. Steinberg, "Research update: report from a workshop on cell biology of retina detachment," Exp. Eye Res. **43**, 695-706 (1986).
39. C. A. Curcio, K. R. Sloan, O. Packer, A. E. Hendrickson, and R. E. Kalina, "Distribution of cones in human and monkey retina: individual variability and radial asymmetry," Science **236**, 579-582 (1987).
40. J. J. Plantner, C. Jiang, and A. Smine, "Increase in interphotoreceptor matrix gelatinase A (MMP-2) associated with age-related macular degeneration," Exp. Eye. Res. **67**, 637-645 (1998).
41. R. H. Steinberg, S. K. Fisher, and D. H. Anderson, "Disc morphogenesis in vertebrate photoreceptors," J. Comp. Neurol. **190**, 501-508 (1980).
42. K. O. Long, S. K. Fisher, R. N. Fariss, and D. H. Anderson, "Disc shedding and autophagy in the cone-dominant ground squirrel retina," Exp. Eye Res. **43**, 193-205 (1986).
43. W. Gao, B. Cense, Y. Zhang, R. S. Jonnal, and D. T. Miller, "Measuring retinal contributions to the optical Stiles-Crawford effect with optical coherence tomography," Opt. Express **16**, 6486-6501 (2008) http://www.opticsinfobase.org/abstract.cfm?URI=oe-16-9-6486.
44. R. J. Zawadzki, B. Cense, Y. Zhang, S. S. Choi, D. T. Miller, and J. S. Werner, "Ultrahigh-resolution optical coherence tomography with monochromatic and chromatic aberration correction," Opt. Express 16, 8126-8143 (2008), http://www.opticsinfobase.org/abstract.cfm?URI=oe-16-11-8126.

1. Introduction

In the last decades, ophthalmoscopy has experienced a genuine explosion of different techniques aimed at increasing the ability to image subtle details in the living retina. This interest is sensible with the fact that blindness in developed countries is mainly caused by retinal pathologies [1]. Early diagnosis of retinal pathologies allows for effective treatment in a number of cases - at least delaying, stopping, or even reversing disease progression. Consequently, the development of ophthalmic techniques able to detect early pathologic retinal changes plays an essential role in ophthalmology. One of the most remarkable advances in the field of high resolution retinal imaging has become possible by the application of adaptive optics (AO) to the human eye, permitting real-time correction of optical aberrations. The correction is mandatory due to the poor optical quality of the eye when using large entrance pupils [2,3].

Optical coherence tomography (OCT) has been incorporated to the increasing list of ophthalmic techniques benefiting from the use of AO. OCT is an imaging modality based upon low coherence interferometry, enabling high axial image resolution [4]. Consequently, applying AO is very attractive for increasing transverse resolution. When using light sources with spectral bandwidths broader than ~80nm, the technique is usually referred to as ultrahigh resolution (UHR) OCT [5]. Axial resolutions of up to 2-3μm have been demonstrated in the human retina with UHR OCT, using light sources emitting 120nm full width at half maximum in the near IR, providing a unique tool for in vivo investigation of retinal architecture [6-8]. The merge of AO and ophthalmic UHR OCT has experienced notable advances in the last few years, possibly driven by the enormous potential of the technique for early medical diagnosis of retinal conditions. The first implementation of the concept (published in a peer-reviewed journal) was in 2004 [9]. One remarkable step forward in the field of OCT was the

#96661 - $15.00 USD Received 27 May 2008; revised 6 Jul 2008; accepted 7 Jul 2008; published 9 Jul 2008

implementation of the commonly named Fourier, spectral, or frequency domain modality. The technique provided notable advantages for ophthalmic applications in terms of efficiency and hence in sensitivity and data acquisition speed [10-14], enabling volumetric mapping of the living retina at high sampling rates. Using this approach, several groups further demonstrated the benefit of merging AO and OCT [15-19]. Other groups also demonstrated the benefits of adaptive optics in combination with systems capable of simultaneous operation of OCT and scanning laser ophthalmoscope [20-22].

In spite of the efforts for increasing transverse resolution applying adaptive optics to OCT in the last years, both by using better correctors and faster image acquisition systems, there appears to be fundamental limitations. Loosely related to this issue, it was reported [17], however, a lack of benefit in the quality of retinal images when correcting monochromatic aberrations by using AO in large pupils combined with ultrabroad spectral bandwidth light sources (140nm FWHM). Following these findings, it was hypothesized [23] about the nature of this effect, modeling the influence of ocular chromatic aberration, spectral bandwidth and entrance pupil size over retinal OCT image quality. In essence, it was found that in the context of OCT imaging, longitudinal ocular chromatic aberration should be compensated for large spectral bandwidths and wide entrance pupils, in order to obtain the expected benefits in resolution from the use of AO [23]. In a subsequent work, an achromatizing lens capable of compensating the average chromatic aberration of the human eye in the near IR range was proposed and demonstrated [24]. Moreover, the lens was successfully implemented in an AO system demonstrating pancorrection in human eyes i.e. full aberration correction [25].

In the current work, we present OCT images with an enhanced level of detail and contrast, showing morphological features in the range of ~2μm in the living human retina, obtained by combining for the first time, pancorrection with UHR OCT. By subjective comparison of AO OCT tomograms with histology, certain questions pertaining to the visualization of photoreceptors in the context of UHR OCT have been addressed.

2. Methods

2.1. Experimental system

The experimental setup (depicted in Figure 1) consisted of two different parts: the AO system, responsible for pancorrection, and the UHR OCT interferometer. The AO system was compounded by spherical mirrors and positive lenses. Those were combined for conjugating the eye's entrance pupil with different planes to be described in the following. The use of mirrors avoided losses of light produced by back reflections. However, off-axis use of spherical mirrors also introduced additional static aberrations, mainly astigmatism and coma aberration. In the system, we combined both lenses and mirrors to achieve a compromise between optical quality and energy losses. The wavefront sensor was a commercially available (HASO 32 EYE) Hartmann-Shack aberrometer, that consisted of an array of square microlenses of 110μm width [26,27]. The number of microlenses sampling the wavefront during the measurements was ~700. Zernike polynomials were retrieved for subsequent correction by the system up to the sixth order. Maximum acquisition frequency of the sensor was 30Hz. The sensor was located at a plane conjugated with the entrance pupil of the eye, indicated as P_0 and P_3 in Figure 1, respectively.

2.2. Deformable mirror

The correcting device was a continuous deformable mirror, capable of modifying its surface for compensating the monochromatic aberrations distorting the wavefront. The deformable mirror (Mirao52, Imagine Eyes, France) used a relatively novel technology with a unique performance in terms of the amplitude and linearity of the deformation. To the best of our knowledge, this type of corrector was used for the first time for retinal imaging in the current work. The principle of operation of the correcting device can be summarized as follows: a set of 52 independent magnets placed beneath the mirror exert a magnetic force deforming the flexible mirrored membrane. The amplitude of the deformation was up to ± 50μm, fully

#96661 - $15.00 USD Received 27 May 2008; revised 6 Jul 2008; accepted 7 Jul 2008; published 9 Jul 2008

covering the ranges of aberrations found in the normal human eye. Moreover, the amplitude also allowed for correcting aberrations from pathologic eyes, known to be affected with larger amounts of aberrations [25]. The control of the mirror was accomplished through the previous measurement of its influence functions [28].

2.3. Achromatizing lens

An essential component of the AO system for pancorrection was the achromatizing lens. A triplet made of standard optical glasses was placed in a plane optically conjugated with the eye's pupil (P_1). The lens was specifically designed for introducing the opposite average value of ocular chromatic aberrations in the near infrared [29]. The triplet was located before the scanning mirrors. This particular position presented the advantage of a steady beam passing through. This fact was of importance since the achromatizing lens might induce lateral chromatic aberration when the incident light is angled with respect to its optical axis [24].

2.4. Interferometer and dispersion compensation

Retinal images were obtained by means of a fiber optically based Michelson interferometer. A compact prism-less mode-locked Titanium:sapphire laser was coupled to the imaging system [30] for illumination. The laser operated at a repetition rate of 110 MHz with a bandwidth of 140nm (full width at half maximum, nearly Gaussian shape) centered at 800 nm, resulting in an axial resolution of ~2μm in tissue. In order to stretch the pulse duration, light from the laser source was launched into a 100m long monomode optical fiber. Taking into account that the laser operates at a repetition rate of 110MHz, light emerging from the fiber can be considered as a continuous wave. This was of a practical importance for calculating retinal exposure limits [31]. The OCT system acquired volumetric information in a series of single depth scans. To form a tomogram (B-mode scan) or a volume, the beam was laterally translated. The beam was raster-scanned by using a pair of galvanometric mirrors (Cambridge

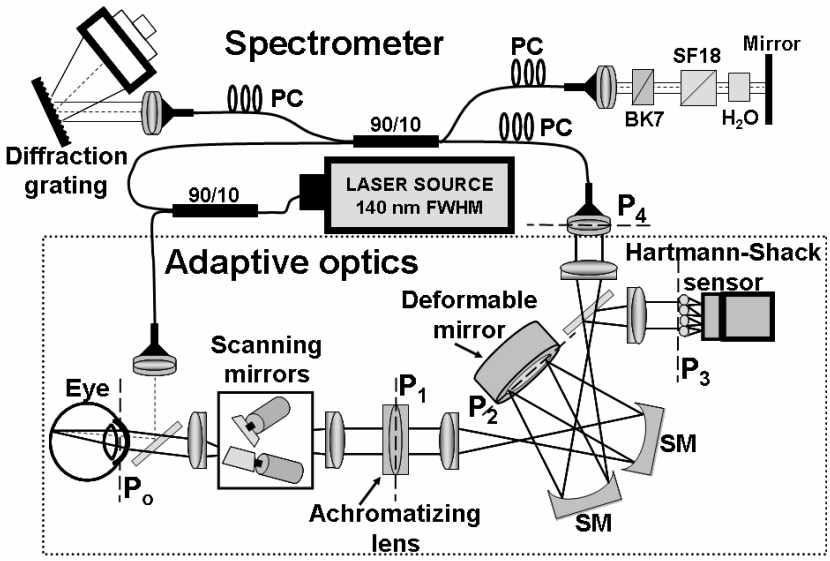

Fig. 1. Experimental system consisting of two parts: an adaptive optics (AO, in dashed lines) system responsible for pancorrection of ocular optical aberrations, and a frequency domain based OCT system for high speed retinal imaging. Charged coupled device (CCD), polarization controller (PC), borosilicate-crown glass (BK7), silicate fluoride (SF18), H_2O (water), conjugate planes of the AO system (P_x), fiber optical beam splitter with 90-to-10% splitting ratio (90/10).

Technologies, USA), placed in planes optically conjugated with the eye's entrance pupil. In this particular set-up a spectrometer consisting of a collimation unit, a grating and a focusing portion were utilized in conjunction with a high speed linear CCD array (ATMEL M2,

#96661 - $15.00 USD Received 27 May 2008; revised 6 Jul 2008; accepted 7 Jul 2008; published 9 Jul 2008

CameraLink 2048 px, 10 klines/s). A high resolution tomogram (e.g., 512x1024 pixels image) was scanned in ~0.1 s. Because of the larger delay for a larger stack of cross-sections, motion artifacts arose along the slow axis. Artifacts due to movements between the B-scans were compensated by cross-correlation and shifting, assuming only small changes between neighbored A-scans. For 3-D representation the resulting stack of images was rendered using Maxon Cinema 4D (version 9).

Appropriate dispersion compensation could be achieved by using the exact amount of optical material in the sample and in the reference arm. However, in practice, this approach is not reasonable when complicated systems involving a large number of optical elements are used. In this work, only two optical glasses were incorporated in the reference arm, BK7 and SF18, to compensate for all the different glasses compounding the lenses in the sample arm. Appropriate thicknesses for these two materials were calculated by using a program, which simulates and compares chromatic dispersion in reference and sample arms. The dispersion introduced by the eye was compensated by adding a 22 mm column of water in the reference arm.

2.5. Experimental protocol and histological preparations

Two subjects, aged 30 and 39 years participated in the measurements. The subjects presented refractions below 0.75 D and no retinal conditions. Accurate positioning and stabilization of the subjects was performed by using a plastic mold with their dental impression and a headrest. Eyes were artificially dilated with cyclopentolate 0.5 %. Closed-loop aberration correction was accomplished at 8 Hz, through an eye's entrance pupil of 6.6 mm diameter. After aberration correction, retinal images were acquired by the OCT system. The power of the illuminating beam was kept below 800μW at the cornea, well matching safety standards of maximum laser exposure [31].

For histological comparison, cryo-sections (thickness 15 μm) were obtained from the foveal region of an isolated corneal transplant donor retina, immunolabeled for short wavelength sensitive (S) cone opsin photopigment. As the S-cone photoreceptors comprise only a minor (> 10%) subpopulation, their single profiles clearly stand out in micrographs and allow visualizing cytological substructures.

3. Results

Three-dimensional images of 260x220x400μm (transverse[x] x transverse[y] x axial[z]) centered at different eccentricities, ~1.12 and ~2.25 degrees nasal, were recorded. Sample spacing of 0.35x0.7x0.75μm was used resulting in 512 x 90 x 550 pixels. The whole investigated retinal volume, equivalent to more than 25 megavoxels, was imaged within ~4 seconds, with the used depth (A)-scan rate of 10000A-scans/second.

Figure 2 shows the benefits of pancorrection in UHR OCT. On top (a-c), three retinal images are displayed, obtained from the same healthy subject through an entrance pupil of 6.6mm diameter and at a retinal eccentricity of ~ 2.25deg nasal. Tomograms were post-processed solely by applying a low pass filter of 2 pixels. Figure 2(a) depicts the case affected by natural ocular aberrations. The image still allowes for resolving most of the intraretinal layers. Figure 2(b) was obtained under monochromatic aberration correction, solely using the deformable mirror. Comparing this image with that previously described, there is a significant increase in signal to noise ratio, allowing for a better visualization of the retinal architecture. Figure 2(c) was obtained using pancorrection of ocular aberrations (i.e., implementing the achromatizing in the setup as well as AO). It is noteworthy, that different dispersion compensation was used for cases b and c. Comparing images b and c, focusing the attention at the visibility of the distinct retinal layers, no significant improvement in the perceived quality of the frames is obvious. Nevertheless, a more detailed view of the photoreceptor layer reveals a notable benefit in case of pancorrection. Areas selected with dashed rectangles in frames a-c (approximately 230μm width) are enlarged in Figs. 2(d-f) enclosing a small portion of the retina between the external limiting membrane and the retinal pigment epithelium (RPE). From d to f, the images correspond to the case of natural aberrations, monochromatic

#96661 - $15.00 USD Received 27 May 2008; revised 6 Jul 2008; accepted 7 Jul 2008; published 9 Jul 2008

aberration correction and pancorrection, respectively. In Fig. 2(d) (from 2(a)), with no aberration correction, morphological structures were barely noticeable. Still, at the photoreceptor level, a set of tenuous and discontinuous spots are visible, perhaps corresponding with individual photoreceptors. In Fig. 2(e) (from 2(b)), morphological features of round shapes are visible at the level of the inner/outer segment junctions (IS/OS PR). According to their size and location, these might correspond to end tips of inner segments of individual photoreceptors, in particular cones. In this case, direct counting was possible. When applying pancorrection, depicted in Fig. 2(f) (from 2(c)), the photoreceptor layer exhibit a different appearance. Elongated structures appeared in the vecinity of the IS/OS PR, recorded as rounded spots with standard AO, became elongated with pancorrection. This shape resembles the true axial morphology of cones as known from histological studies, exhibiting conical and elongated shapes, arranged nearly parallel to each other. In Fig. 2(e), when pancorrection was applied, several morphological elements can now be clearly assigned to cone photoreceptor substructures.

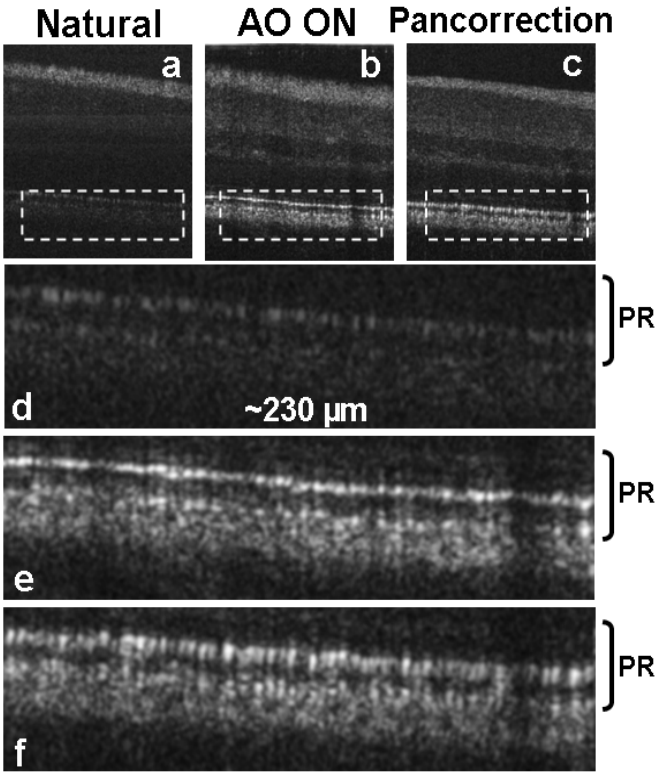

Fig. 2. Effect of pancorrection: three retinal tomograms obtained from a normal subject through an entrance pupil of 6.6 mm diameter, at ~2.25 deg nasal. Case affected by natural ocular aberrations (a), monochromatic aberration correction (b), pancorrection (c). Enlarged areas are from the level of the inner/outer segment junctions (IS/OS PR) to the retinal pigment epithelium (d, e, f from a, b, and c, respectively).

Figure 3 compares retinal sections obtained with pancorrection in a normal subject at ~1deg (a, d) and ~2deg (c, f) with cryosections of adult human retinas with anti-S-opsin DAB-labeling: a DIC micrograph of 15µm (centered at ~250µm eccentricity) labeled for S-opsin to reveal the minority of short wavelength sensitive cones (b) and a sum projection of a focus series (~500µm-eccentricity) revealing entire S-cone profiles (e). As separate elements with

#96661 - $15.00 USD Received 27 May 2008; revised 6 Jul 2008; accepted 7 Jul 2008; published 9 Jul 2008

clear axial continuities are identifiable, direct correlations of the individual photoreceptor signals in OCT with corresponding photoreceptor elements from histology can be established.

In Fig. 3(a) it can be noticed that nuclear layers scatter light less than those compounded by nerve fibers, dendrites (plexiform layers) or membrane-rich organelles (mitochondria, photoreceptor outer segments). The distal retinal layers corresponding to the photoreceptors and RPE feature the strongest signals (a, c). An enlarged (4x) part of the photoreceptor area (d, f) depicts the unique resolution and contrast of the images achieved, allowing to objectively identify and distinguish individual photoreceptors and several of their sub-elements can be correlated to high resolution light microscopy as exemplified in a micrograph and drawing (e). Accounting for the retinal eccentricity of the measured volumes, the photoreceptors must correspond mainly to cones. Below the external limiting membrane (ELM), a clear bipartition is present between a coarser distal speckle pattern of the cell bodies (CB) of the outer nuclear layer (ONL) and a finer proximal texture, probably originating from the radiating cone axons (Henle-fibers, HF). The ELM is represented by a thin linear OCT

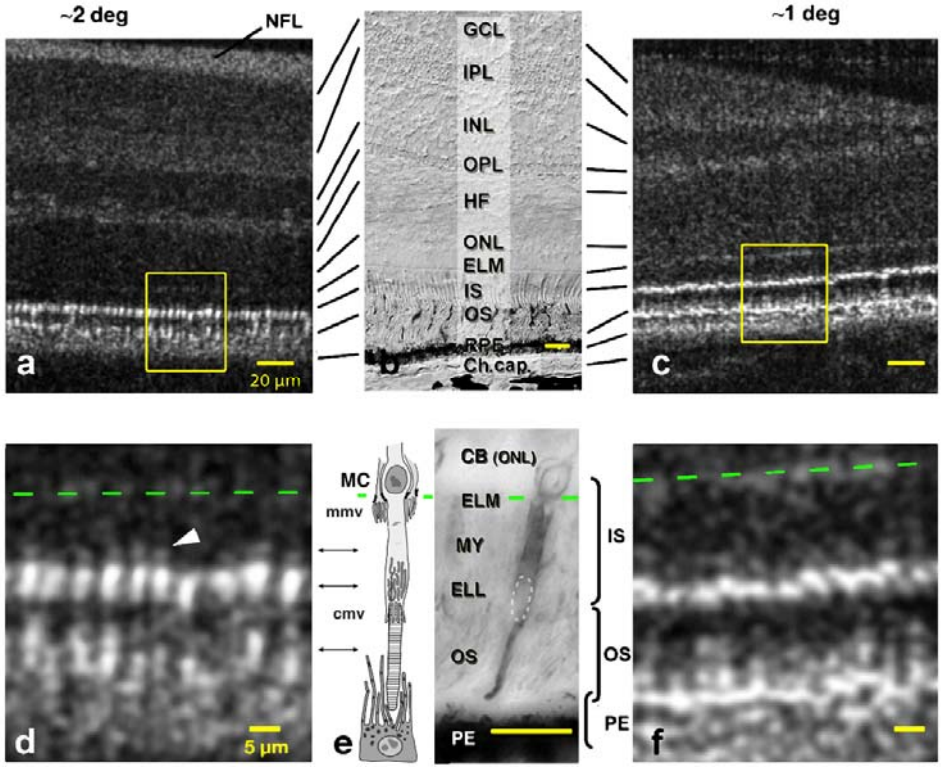

Fig. 3. AO OCT retinal imaging using pancorrection in a normal subject at two nasal parafoveal locations, at ~ 2 deg (a, d) and ~ 1 deg (c, f), and micrographs of 15 µm cryosection of an adult human retina with visualization of short wavelength sensitive cones by opsin antibody: differential interference contrast (DIC) profile at ca. 250 µm eccentricity (b), and a sum projection at ca. 500 µm eccentricity (e), outlining the characteristic axial organization of cone profiles (e), as exemplified in the adjacent schematic drawing. At ~2 deg the enlarged (4x) distal portions of the OCT profiles (d) obtained with pancorrection allows to objectively distinguish individual photoreceptors and several of their axial elements: ellipsoid (ELL) and myoid (MY, arrowhead points to distinct distal portions) of the cone inner segments (IS) and a second high intensity sub-tier clearly represents the photoreceptor outer segment (OS) zone. The next evident layers represent the retinal pigment epithelium with processes (surrounding outer segment tips) and the epithelial cellular portion. At ~1 deg (c, f), in spite of smaller cone diameters as compared with higher eccentricities, imaging different distal parts of individual photoreceptors is still partly possible. Cone cell bodies (CB), Müller cell (MC) and ELL microvillar zone (mmv, cmv), nerve fiber layer (NFL), ganglion cell layer (GCL), inner plexiform layer (IPL), outer plexiform layer (OPL), Henle fiber layer (HF), outer nuclear layer (ONL), external limiting membrane (ELM) is indicated by green dashes in d)-f), ELL by white dashes in e), retinal pigment epithelium (R/PE), choriocapillaris (Ch.cap.).

#96661 - $15.00 USD Received 27 May 2008; revised 6 Jul 2008; accepted 7 Jul 2008; published 9 Jul 2008

signal. Its discontinuous structure (dashed green line in Fig. 3(d,e,f)) could be related to its structural and optical complexity: cone myoids, emerging from the ONL, are surrounded by Müller cell (MC) junctions. Additionally, collars of Müller cell microvilli (mv', 4µm), largely fill the inter-receptor space [32] shifting complete optical separation of cones towards more distal inner segment levels. Above this low intensity speckle, elongated medium density myoidal signals (~3-4µm width, arrowhead) become discernible at ~6-7µm above the ELM, extending further (4-5.5µm) before becoming distally attached to axially corresponding bright cylindro-elliptical signals. These signals correlate with the distal portions of cone inner segments, the ellipsoids (ELL, outlined in micrograph), consisting of densely packed tubular mitochondria with multiple internal membranes (cristae). For their high refractive index ELL are discussed to optically serve as micro-lenses [33,34].

While the inner segments of foveolar cones are essentially tubular, the ellipsoids of extrafoveolar cones have increased diameters compared to both the proximal myoids and the outer segments distally, and thus determine the cone diameters and intercone distances. At ~2° eccentricity, ellipsoid diameters are ~2.5-5.4µm with ~5.4µm mean spacing, being in close accordance with intercone distances reported from histological studies [35].

Distal to the ellipsoidal tips, a zone of relatively low signal intensity follows. As known from microscopy [32,36], this level represents the ciliary base of the outer segments and a collar of ellipsoidal microvilli (mv''). Distally this connecting zone attaches to intense cylindrical signals evidently corresponding to cone outer segments (OS). The OS are not always included completely in the scanned volume, probably due to their thinner diameter and possibly to some axial jitter [37]. Distal portions of the OS are embedded within pigment epithelial (PE) processes. The granulose texture there may originate from melanin and lipofuscin granules, phagosomes and residual bodies [38], expected to significantly decrease the recorded OCT signal as well as from longer rod outer segments. Figures 3 (c,f) show a section closer to the foveal center (1°eccentricity). Figure 3(f) reveals more densely packed cones with separations between adjacent units in the order of 2-3µm [39]. Pancorrected AO-OCT still allows for visualizing different distal parts of these photoreceptors. In Fig. 3 (d,f), individual ellipsoids are distinguishable. A more distinct transition zone to the PE possibly results from the uniform length of cone OS and the near complete lack of interspersed rod OS

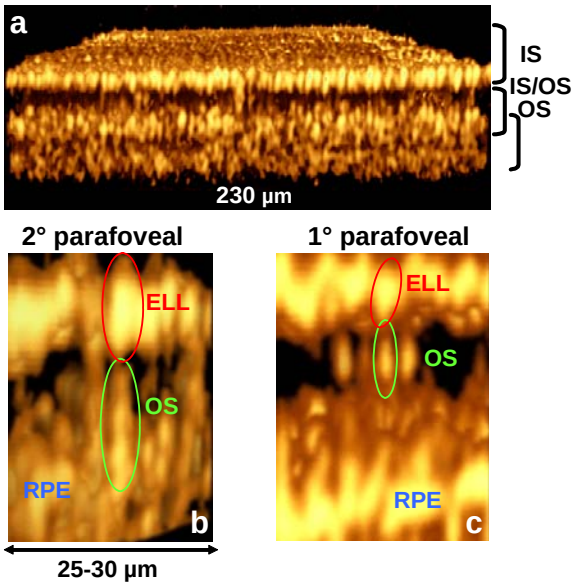

Fig. 4. *In vivo* cellular resolution retinal imaging: three-dimensional OCT using pancorrection of a small retinal volume, at ~2.25 deg eccentricity, of 230 µm lateral extension obtained (a). Three-dimensional morphology of photoreceptor ellipsoids, together with the outer segments, is visualized. Two different volumes showing the detailed micro-structural architecture of single photoreceptors at two eccentricities: ~2,25 and ~1,12 deg (b, c).

#96661 - $15.00 USD Received 27 May 2008; revised 6 Jul 2008; accepted 7 Jul 2008; published 9 Jul 2008

at this eccentricity. Interestingly, some of the ellipsoids in the figure exhibit a skewed orientation other than expected, deviating from the direction of the incoming light. OS are also visible, appearing as elongated cylinders.

Aside from cross-sections, the pancorrected AO-OCT also permitted true three-dimensional retinal imaging with isotropic resolution. Figure 4 depicts a retinal volume, obtained at ~2.25deg eccentricity, of 230µm lateral extension. The distal part of the retina covering the OS of the photoreceptors was selected. The gold pseudo-color was used to enhance the contrast and appearance of this volumetric rendering. In Fig. 4(a), the three-dimensional structure of the ellipsoids, together with the OS, was recognizable. The detailed study of the volume revealed the three-dimensional morphology of the photoreceptors in the living eye. In Figs. 4(b, c), two different small volumes of only 25-30µm transverse extension were presented, showing the micro-structural architecture of individual photoreceptors at two eccentricities: 2.25 and 1.12deg, respectively.

In vivo volumetric investigation of the human retina at cellular resolution might permit to unveil early micro-structural morphological changes. In this context, when using UHR-OCT with pancorrection, some interesting structural features in the foveal region were recorded, and are presented in Fig. 5. The structures appeared throughout adjacent images, indicating that they corresponded to real morphological details rather than imaging artifacts. Fig.5 (a) shows an example of these features at a retinal location ~265µm nasally, with a lateral size of ~130µm. A dashed square emphasizes a ~50µm lateral retinal portion, containing the zone between ELM and RPE. Close to the IS/OS PR, in the OS region and towards the RPE, there were two circular features of low reflectance. An additional one was found ~70µm nasally, again close to IS/OS PR but towards the vitreous in this case instead, likely in the ellipsoid of the IS. The three spots are marked in Fig. 5(a) with white arrows. Four consecutive, adjacent and enlarged tomograms are presented in Figs. 5(b-e) with 0.7µm transverse separation. The diameter estimated for these low scattering structures was ~3-4µm. Since they could be clearly identified across 7 adjacent images at nearly the same location within each image, it can be inferred that they were parallel to each other and horizontally located in the retina with a transverse dimension of at least 5µm. They might be indicators of morphological changes perhaps connected with early stages of some retinal conditions, like macular dystrophy [40]. Additional studies are required to understand the origin and significance of these structures.

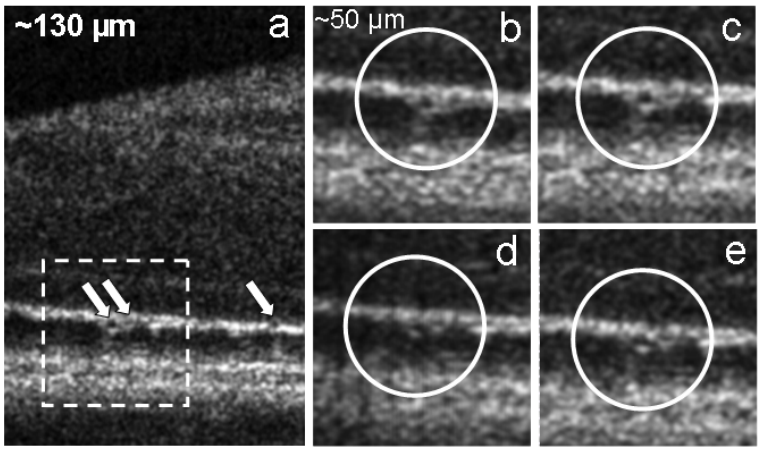

Fig. 5. Cellular resolution retinal imaging of photoreceptor anomalies: tomogram centered at ~ 265 µm nasally from the foveal center with a dashed square of a small portion of the retina, ~ 50 µm lateral, containing the zone between external limiting membrane and retinal pigment epithelium. Two dark grey circular features in four consecutive, adjacent and enlarged tomograms at this location (b-e) that might be indicators of early changes, such as neovascularization, in the photoreceptor layer.

#96661 - $15.00 USD Received 27 May 2008; revised 6 Jul 2008; accepted 7 Jul 2008; published 9 Jul 2008

4. Discussion

The main limitation for visualization of the intraretinal architecture is the intrinsic low reflectance of certain layers. The use of pancorrection might increase OCT contrast and resolution by enabling a more efficient concentration of the scanning beam on the retina, and also on the detector after photons have been backscattered by the retinal tissue. In addition, correction of ocular achromatic aberration might allow for applying light sources with even broader spectra, beyond 140nm, further improving OCT axial resolution in the living human retina.

Since the reflectance or the capability to scatter incident light are expected to be essentially similar across normal subjects, the change in the appearance of images must be mainly due to the focusing properties of the illuminating beam sampling the retina, and the better concentration of energy in the detector. Pancorrection enables tightly focused polychromatic beams at the focal plane in the living human retina. Given that the amount of energy delivered in the retina must stay within safety exposure limits [31], it is expected that other layers of the retina further away from the focal plane are recorded with decreased sensitivity as compared to those recorded without pancorrection.

In the present work, three-dimensional *in vivo* imaging of individual photoreceptor outer segments is presented (Fig. 3 and 4). This imaging modality opens the door to study the possible connection between pathologies associated to the loss or alteration of photoreceptor elements, including the internal process of renewing photoactive discs. In this context, the inhomogeneous appearance of the signal obtained from OS in this work, was noticeable. Outer segments are not surrounded by empty space but rather embedded in a meshwork of extracellular material, the so-called inter-photoreceptor matrix. Furthermore villous processes of pigment epithelial cells containing or lacking pigment (melanin) granules establish a cylindrical curtain around outer segments involved in many processes including retinoid metabolism, light screening and phagocytosis [41,42]. Monitoring this part of the cell is fundamental for the early diagnosis of some retinal conditions associated with the photoreceptor pigment epithelial interface, such as drusen.

In Fig. 3(d, f) some portions of the distal ellipsoid layers appear to have different tilts,. This indicates that identification of misalignment of photoreceptors and in vivo characterization of the Stiles-Crawford effect is becoming possible. Recently, the use of OCT has been reported for Stiles-Crawford investigation [43]. Notably, in our work larger intercone spaces are present between cones at 2°eccentricities (Fig. 2) while rod photoreceptors were not evidently recognizable, It is possible that their diameters, and light guiding properties did not lend themselves to discrete signals.

Also, differences in cone appearance between 1° and 2° may not solely be attributable to the smaller diameters. As noted by Hoang et al. [33], the mitochondria of parafoveal cones tend to be concentrated in the distal IS, while in foveal cone segments they are more dispersed, often extending to the outer fibers of the ELM. Such differences may influence the appearance of related structures and possibly induce axial dimensional anisotropies in pancorrected UHR OCT.

An interesting issue is the depth of focus achieved with this novel modality. The problem has been studied in the context of OCT in the reference 18. The scattering properties of the human retina are not well understood, even with ex vivo samples. This is of huge importance when the problem involves a broad spectral range (in the current work 140 nm FWHM), due to the strong dependence of scattering with wavelength. When using relatively short spectral bandwidths (as it is the case in ref. 18) calculations might be programmed solely considering the central wavelength. In our case, the ultra broad spectrum introduced in the eye maked theoretical calculations out of the scope of this work due to the lack of a model of the scattering properties of the human retina in the spectral range employed in our measurement. Still, solely under ideal conditions and in order to provide an order of magnitude, it could be assumed that a light spot of size 2 μm sampling the retina is distributed along a light cone of

#96661 - $15.00 USD Received 27 May 2008; revised 6 Jul 2008; accepted 7 Jul 2008; published 9 Jul 2008

20 μm. Out of this distance, the scanned beam is rapidly increasing its diameter, consequently losing resolution and contrast.

Recently, an interesting work has been published combining monochromatic and chromatic ocular aberration correction and OCT [44]. The core of the image modality is similar to the one presented in the current manuscript, although both works present significant differences in the implementation of the technique. Among others, the incorporation of the achromatizing is differently accomplished. In Zawadzki's work [44] a triplet is specifically designed for their setup, to be located at the entrance of the sample arm. This way largely solves the problem of back reflection on the wavefront sensor, making however the adaptation of the achromatizing lens impossible to other setup. In our paper, we designed the achromatizing triplet to be placed at a conjugate plane of the entrance pupil of the eye with absolute magnification of 1. This approach requires the use of an additional conjugated plane in the system, but makes it possible to use the triplet in any setup, or even directly in front of the eye. In addition, probably due to the wider spectral bandwidth employed in the current work, retinal images appear with fewer speckles as compared with reference 44. Consequently, morphological details are more evident. In particular, the morphology of the photoreceptors, the conic shape of the ellipsoid, is clearly resolved in our images. In reference 44, averaging of several B-scans is performed to reduce the effect of speckle. Although the quality of the retinal images is lower, this approach could be of huge interest in low cost systems, since the operation is performed by appropriate software and there is no need of light sources of emitting wider spectrum. However, the use of several B-scans prevents for three-dimensional representations of the retinal tissue as previously presented in this work.

In summary, these observations demonstrate that descriptions of individual photoreceptors have become possible. The novel technique demonstrated in the present work could provide additional and more specific information about the pathogenesis and evolution of some conditions and eventually, and before changes are detectable with standard clinical diagnostic methods. For instance, a variation in the density and alignment of outer segments, which can be studied at selected eccentricities in the living retina, might be an early indicator of conditions associated with the loss of photoreceptors. The imaging method has the potential for studying individual photoreceptors, providing a unique method to non-invasively monitor the effects of certain drugs or pathologies at cellular resolution. Furthermore, a semi-quantitative estimation of organelle volumes such as ellipsoidal mitochondria may become possible to monitor and study related diseases in vivo.

Acknowledgments

We gratefully acknowledge support from L. Vabre, X. Levecq and N. Chateau, Imagine Eyes, Orly, France, C. Glittenberg, S. Binder, Department of Ophthalmology, Ludwig Boltzmann Institute Rudolf Foundation Clinic Vienna, Austria and Maxon Computer GmbH. This work was supported in part by Cardiff University, FWF P14218-PSY, FWF Y 159-PAT, CRAF-1999-70549 as well as the Christian Doppler Society.

#96661 - $15.00 USD Received 27 May 2008; revised 6 Jul 2008; accepted 7 Jul 2008; published 9 Jul 2008